The Astrophysical Journal, 798:56 (9pp), 2015 January 1 doi:10.1088/0004-637X/798/1/56

AN ULTRA-LOW-MASS AND SMALL-RADIUS COMPACT OBJECT IN 4U 1746-37?

Zhaosheng Li[1], Zhijie Qu[1], Li Chen[2], Yanjun Guo[1], Jinlu Qu[3], and Renxin Xu[1,4]
[1] School of Physics and State Key Laboratory of Nuclear Physics and Technology, Peking University, Beijing 100871, China; lizhaosheng@pku.edu.cn
[2] Department of Astronomy, Beijing Normal University, Beijing 100875, China
[3] Laboratory for Particle Astrophysics, Institute of High Energy Physics, CAS, Beijing 100049, China
[4] Kavli Institute for Astronomy and Astrophysics, Peking University, Beijing 100871, China
Received 2014 May 14; accepted 2014 October 24; published 2014 December 19

ABSTRACT

Photospheric radius expansion (PRE) bursts have already been used to constrain the masses and radii of neutron stars. *RXTE* observed three PRE bursts in 4U 1746-37, all with low touchdown fluxes. We discuss here the possibility of a low-mass neutron star in 4U 1746-37 because the Eddington luminosity depends on stellar mass. With typical values of hydrogen mass fraction and color correction factor, a Monte Carlo simulation was applied to constrain the mass and radius of a neutron star in 4U 1746-37. 4U 1746-37 has a high inclination angle. Two geometric effects, the reflection of the far-side accretion disk and the obscuration of the near-side accretion disk, have also been included in the mass and radius constraints of 4U 1746-37. If the reflection of the far-side accretion disk is accounted for, a low-mass compact object (mass of $0.41 \pm 0.14\,M_{\odot}$ and radius of 8.73 ± 1.54 km at 68% confidence) exists in 4U 1746-37. If another effect operated, 4U 1746-37 may contain an ultra-low-mass and small-radius object ($M = 0.21 \pm 0.06\,M_{\odot}$, $R = 6.26 \pm 0.99$ km at 68% confidence). Combining all possibilities, the mass of 4U 1746-37 is $0.41^{+0.70}_{-0.30}\,M_{\odot}$ at 99.7% confidence. For such low-mass neutron stars, it could be reproduced by a self-bound compact star, i.e., a quark star or quark-cluster star.

Key words: binaries: general – stars: individual (4U 1746-37) – stars: neutron – X-rays: binaries – X-rays: individual (4U 1746-37) – X-rays: stars

1. INTRODUCTION

The equation of state (EoS) of superdense matter is one of the key questions in astrophysics and nuclear physics. Neutron stars (NSs; hereafter "NS" refers to all kinds of pulsar-like compact objects) in the universe provide us with a unique opportunity to approach it. Generally, two categories of EoS were widely discussed, which can produce gravity-bound NSs and self-bound NSs (Glendenning 1996; Haensel et al. 2007), respectively. All of them proposed distinct mass–radius relations. The EoSs of self-bound NSs predicted $M \propto R^3$ (M and R are the mass and radius of NSs, respectively) for low-mass NSs. Moreover, the minimum mass of self-bound NSs can reach as low as planet mass (Xu & Wu 2003; Horvath 2012), while the low-limit mass of gravity-bound NSs is about $0.1\,M_{\odot}$ (e.g., Akmal & Pandharipande 1997; Glendenning & Schaffner-Bielich 1999). The measurements of the radius and mass of NSs, as well as searching extremely low-mass NSs, can provide useful information to test various theoretical EoSs.

The mass of NSs can be precisely determined in double-NS systems or white dwarf–NS systems (see Lattimer 2012 for all NSs with measured masses). Especially, Janssen et al. (2008) found a very low mass NS ($<1.17\,M_{\odot}$ at 95.4% confidence) in PSR J1518+4904, which might be the least massive compact object in a double-NS system. The direct measurement of the radius of NSs, however, is still difficult. The measurement of NS radius is very critical for constraining the EoS. Fortin et al. (2014) claimed that the NSs with mass in the range 1.0–$1.6\,M_{\odot}$ should be larger than 12 km; otherwise, the presence of hyperons in NS cores is ruled out. And then, the so-called hyperon puzzle arises (e.g., Bednarek et al. 2012). Several methods were proposed to constrain the radius and mass of NSs, such as fitting the thermal spectra from quiescent low-mass X-ray binaries (LMXBs) in globular clusters (Guillot et al. 2013), simulating X-ray pulsar profiles (Leahy 2004), and photospheric radius expansion (PRE) bursts (see Bhattacharyya 2010 for a review).

Type I X-ray bursts in LMXBs are a sudden energy release process, which lasts tens to hundreds of seconds and can emit as high as Eddington luminosity ($\sim 3.79 \times 10^{38}\,\mathrm{erg\,s^{-1}}$). In the classical view, type I X-ray bursts are powered by the unstable thermonuclear burning of H/He accreted on the NS surface through its companion star Roche lobe overflowing. Most of the spectra of type I X-ray bursts can be well fitted by a pure blackbody spectrum. PRE bursts, a special case of type I X-ray bursts, were phenomenally distinguished from the time-resolved spectra. At the touchdown moment, where the blackbody temperature and its normalization reach their local maximum and minimum during X-ray burst, respectively, the referred bolometric luminosity corresponds to its Eddington luminosity, that is, the radiation pressure is balanced by gravity. After the touchdown point, the residual thermal energy cools on the whole surface of the NS during the burst tail. So, the mass and radius of the NS could be constrained if the distance to the source was measured independently, i.e., in globular clusters (Sztajno et al. 1987; Özel et al. 2009).

Under the assumption of spherically symmetric emission, the Eddington luminosity is expressed as (Lewin et al. 1993)

$$L_{\mathrm{Edd}} = \frac{8\pi G m_p M c[1 + (\alpha_T T_e)^{0.86})]}{\sigma_T (1 + X)(1 + z(R))}, \quad (1)$$

where G, c, and σ_T are the gravitational constant, the speed of light, and the Thomson scattering cross section, respectively; m_p is the mass of the proton; X is the atmosphere's hydrogen mass fraction ($X = 1$ for pure hydrogen); T_e is the effective temperature of the NS atmosphere; and α_T describes the temperature dependence of the electron scattering opacity. The factor $1 + z(R) = (1 - 2GM/Rc^2)^{-1/2}$ is the gravitational

redshift correction for the strong gravity field on the surface of an NS. Kuulkers et al. (2003) analyzed all PRE bursts in globular clusters with known distance and discussed the potential advantage of PRE bursts as "standard candles." Galloway et al. (2008a) argued that the luminosity of PRE bursts was intrinsically affected by the mass and radius of NSs, the variation of photosphere composition. Especially, two low-luminosity sources during PRE bursts, 4U 1746-37 and GRS 1747-312, emitted too faintly to reach Eddington luminosity under the assumption of $1.4\,M_{\odot}$. However, the possibility of the observed low flux due to the existence of low-mass NSs, i.e., $0.7\,M_{\odot}$ (Sztajno et al. 1987), cannot be ruled out.

We interpret that a low-mass NS inside 4U 1746-37 and GRS 1747-312 can explain their low touchdown fluxes in PRE bursts. However, a peculiar X-burst from GRS 1747-312 exhibited significant variation of apparent radius in the cooling tail (in't Zand et al. 2003). The color correction factor and emission area may simultaneously change similarly to the case in 4U 1820-30 (García et al. 2013). In this work, we only discuss the possibility of a low-mass NS in 4U 1746-37.

Compared with very early works by Sztajno et al. (1987), we consider the touchdown fluxes, instead of peak fluxes, observed by *RXTE* in 4U 1820-30 as its Eddington flux. Moreover, the reflection or obscuration by accretion disks is accounted for separately (Galloway et al. 2008b). The accretion rate enhancement during X-ray bursts is checked (Worpel et al. 2013; in't Zand et al. 2013). The effects of an extremely extended photosphere at the touchdown moment are also investigated (Steiner et al. 2010).

In Section 2 the *RXTE* observations of 4U 1746-37 are briefly presented. In Section 3 we introduce the mass–radius constraints of 4U 1746-37. We give the results and discussions in Sections 4 and 5, respectively.

2. *RXTE* OBSERVATIONS

During its 15 yr in operation, *RXTE* observed over 1000 X-ray bursts, which were analyzed in detail in Galloway et al. (2008a). The high-quality data provided an opportunity to research the time-resolved spectra of X-ray bursts. The PRE bursts, a special type of X-ray bursts, emitted Eddington luminosity and cooled on the whole surface of NSs with small uncertainties (Güver et al. 2012a, 2012b), which were utilized to determine the M and R of NSs (Özel et al. 2009, 2012; Güver et al. 2010a, 2010b). The dominant uncertainties of M and R originated from the error of the distance to source (Sala et al. 2012).

The touchdown fluxes and blackbody normalizations (A) were obtained in the time-resolved spectra of PRE bursts. When extracting the time-resolved spectra, several assumptions were made first (Worpel et al. 2013). The spectra of persistent emission during bursts were stable and invariant. The net contribution of a burst was archived by subtracting its preburst intensity, which arose from accretion. in't Zand et al. (2013) observed a type I X-ray burst in SAX J1808.4-3658 with *RXTE* and *Chandra* simultaneously and found obvious excess of low- and high-energy photons when fitting the burst spectrum with a blackbody. Worpel et al. (2013) explained that the excesses at low and high energies in SAX J1808.4-3658 and other PRE bursts were due to accretion enhancement during the burst, analogous to the Poynting–Robertson drag effect. in't Zand et al. (2013) introduced the "f_a" model to account for the contribution of persistent emission. Worpel et al. (2013) found that for most of the spectra the factor f_a was significantly larger than unity, especially for SAX J1808.4-3658 ($f_a = 17.75$). We check this kind of accretion rate enhancement during type I X-ray bursts in 4U 1746-37.

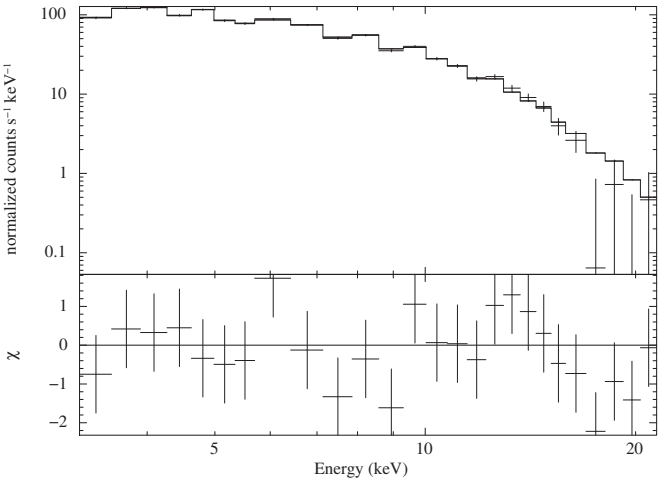

Figure 1. Persistent emission spectrum of 4U 1746-37 (ObsID 30701-11-03-000). The reduced χ^2 is 1.01, which implies a good fitting to the data.

2.1. Data Reduction

4U 1746-37 is an LMXB located in the globular cluster NGC 6441. The distance to NGC 6441 is $11.0^{+0.9}_{-0.8}$ kpc (Kuulkers et al. 2003). From the type I X-ray burst catalog of *RXTE* (Galloway et al. 2008a), three PRE bursts were identified in 4U 1746-37 (ObsID 30701-11-03-000, 30701-11-04-00, and 60044-02-01-03, hereafter cited as Bursts I, II, and III, respectively). In order to check the accretion rate enhancement consequence during type I X-ray bursts (Worpel et al. 2013), we reanalyzed these three PRE bursts of 4U 1746-37, which were collected by the Proportional Counter Array (PCA) on board *RXTE*. The time-resolved spectra were extracted from the appropriate model files (science event or Good Xenon), which covered the whole burst interval in the energy range 2–60 keV. The dead-time corrections were made following the process suggested by the *RXTE* team.[5] We fitted the spectra in the range 3–22 keV and added a 0.5% systematic error. We fixed the hydrogen column density at 0.26×10^{22} cm^{-2} obtained from *BeppoSAX* (Sidoli et al. 2001), which has higher sensitivity at low X-ray energy than *RXTE*/PCA. The dead-time correction factor ranges of each observation are listed in Table 1.

2.2. Persistent Emission

For each PRE burst in 4U 1746-37, a 16 s interval prior to the trigger moment was regarded as persistent emission, which contains emission from the source, as well as background from the instrument. We utilized the "bright" source model (>40 counts s^{-1} PCU^{-1}) to estimate the instrumental background with the *runpcabackest* procedure. The persistent emission can be well fitted by an absorbed blackbody plus power law (wabs(bbodyrad+powerlaw) in Xspec). Figure 1 shows the fit to the persistent spectrum and the residuals of Burst I. The reduced χ^2 is 1.01 for 22 degrees of freedom. For the other two PRE bursts, the reduced χ^2 are 0.98 (Burst II) and 0.82 (Burst III), indicating a good fitting to the data.

[5] http://heasarc.nasa.gov/docs/xte/recipes/pca_deadtime.html

Table 1
PRE Bursts in 4U 1746-37

Obs_ID	Touchdown Flux (10^{-9} erg s^{-1} cm^{-2})	Peak Flux (10^{-9} erg s^{-1} cm^{-2})	DCOR[a]	PCU on[b]	*M–R*
30701-11-03-000	2.86 ± 0.16	4.84 ± 0.25	1.028-1.035	All	$0.21 \pm 0.06\,M_\odot$, 6.26 ± 0.99 km[c]
30701-11-04-00	2.21 ± 0.14	5.23 ± 0.26	1.023-1.030	All	$0.41 \pm 0.14\,M_\odot$, 8.73 ± 1.54 km[d]
60044-02-01-03	3.01 ± 0.13	5.84 ± 0.23	1.015-1.026	0,2,4	

Notes.
[a] Dead-time correction factor (DCOR) range. The exposure time of each burst spectrum is divided by DCOR.
[b] The active Proportional Counter Units (PCUs) during the burst epoch.
[c] The 1σ confidence level of mass and radius NS in 4U 1746-37, corresponding to Figure 6.
[d] The 1σ confidence level of mass and radius NS in 4U 1746-37, corresponding to Figure 7.

2.3. Fitting the Burst Spectra

The net burst spectrum can be represented by a pure blackbody with interstellar absorption. Worpel et al. (2013) introduced an f_a-model to account for the variation of persistent emission amplitude, which is presented as

$$S(E) = A(E) \times B(E; T_{\rm BB}, A_{\rm BB}) + f_a \times P(E) - b(E)_{\rm inst}, \quad (2)$$

where $A(E)$ is the absorption correction, $B(E; T_{\rm BB}, A_{\rm BB})$ is the blackbody spectrum with temperature $T_{\rm BB}$ and normalization $A_{\rm BB}$, $P(E)$ is the persistent emission, and $b(E)_{\rm inst}$ is the instrumental background. The parameter f_a accounts for the contribution from the persistent emission, i.e., $f_a = 1$ means that the amplitude of persistent emission is exactly the same as the moment before the X-ray burst trigger. Note that the f_a model is applied, assuming that only the amplitude of persistent emission can change. The f_a distribution of type I X-ray bursts from the Galloway et al. (2008a) catalog peaks at 1 and is biased toward higher values (Worpel et al. 2013). This implies that the accretion rate increases during X-ray bursts, analogous to the Poynting–Robertson effect.

We also attempted to find whether the persistent emission varied or not in 4U 1746-37. When the f_a model was used, we applied the *f*-test to check the requirement of adding this extra parameter. We found that the f_a model cannot produce distinctly better reduced χ^2. It implies that even if the accretion rate increased during type I X-ray bursts in 4U 1746-37, its contribution to the burst spectrum can be neglected. We generated the time-resolved spectra of three PRE bursts in Figures 2–4. The bolometric flux, the blackbody temperature, the blackbody normalization, and the reduced χ^2 are shown. The bolometric flux was calculated from Equation (3) in Galloway et al. (2008a). The error of bolometric flux was estimated from the uncertainty propagation. All quoted errors are at the 68% confidence level.

In Figure 2 the reduced χ^2 on the cooling tail are relatively large compared with the expansion phase and contraction phase, as with the f_a model. The touchdown fluxes are $(2.86 \pm 0.16) \times 10^{-9}$ erg s^{-1} cm^{-2}, $(2.21 \pm 0.14) \times 10^{-9}$ erg s^{-1} cm^{-2}, and $(3.01 \pm 0.13) \times 10^{-9}$ erg s^{-1} cm^{-2}. The corresponding peak fluxes are $(4.84 \pm 0.25) \times 10^{-9}$ erg s^{-1} cm^{-2}, $(5.23 \pm 0.26) \times 10^{-9}$ erg s^{-1} cm^{-2}, and $(5.84 \pm 0.23) \times 10^{-9}$ erg s^{-1} cm^{-2}. Meanwhile, the factor $F_{\rm p}/F_{\rm TD}$ is 2.0 ± 0.3. If the cooling tails were truncated at 0.5×10^{-9} erg s^{-1} cm^{-2}, we obtained the apparent area during the cooling tail 10.9 ± 4.2 (km/10 kpc)^2, which is smaller than 15.7 ± 2.4 (km/10 kpc)^2 provided by (Güver et al. 2012b), but with a larger error, since we only used three PRE bursts and did not group the apparent areas as a function of flux.

Suleimanov et al. (2011) proposed that the color correction factor apparently changes when the luminosity is close to its Eddington limit. In Figure 5, the $A^{-1/4}$–flux correlation is shown and fitted by three theoretical models (Suleimanov et al. 2012). The data are well fitted at high flux ($F_{\rm TD} = 2.65 \times 10^{-9}$ erg s^{-1} cm^{-2} and $[R(1+z)/D_{10}]^{-1/2} = 0.35$ for pure H, $F_{\rm TD} = 2.7 \times 10^{-9}$ erg s^{-1} cm^{-2} and $[R(1+z)/D_{10}]^{-1/2} = 0.36$ for pure He, $F_{\rm TD} = 2.65 \times 10^{-9}$ erg s^{-1} cm^{-2} and $[R(1+z)/D_{10}]^{-1/2} = 0.37$ for a mixture of H/He). At low flux, the data deviate from the prediction of models, which also appears in GS 1826-24 (Zamfir et al. 2012). Güver et al. (2012b) calculated f_c for different X-ray burst atmosphere models and concluded that f_c is weakly dependent on the temperature if the blackbody temperature is less than 2.5 keV. From the time-resolved spectra of 4U 1746-37, the blackbody temperatures are all in the range 1–2 keV. Hence, the color correction factor is chosen as 1.3–1.4 to account for the different theoretical model predictions.

The standard deviations of $F_{\rm TD}$ and A contain three parts: the observed errors ($\sigma_{F_{\rm TD,obs}}$, $\sigma_{A_{\rm obs}}$), the systematic errors ($\sigma_{F_{\rm TD,sys}}$, $\sigma_{A_{\rm sys}}$), and the absolute calibration errors ($\sigma_{F_{\rm TD,cal}}$, $\sigma_{A_{\rm cal}}$), which are

$$\sigma^2_{F_{\rm TD}} = \sigma^2_{F_{\rm TD,obs}} + \sigma^2_{F_{\rm TD,sys}} + \sigma^2_{F_{\rm TD,cal}} \quad (3)$$

and

$$\sigma^2_{A} = \sigma^2_{A_{\rm obs}} + \sigma^2_{A_{\rm sys}} + \sigma^2_{A_{\rm cal}}, \quad (4)$$

if these errors are independent of each other. Here the 10% absolute calibration errors are applied (Tsujimoto et al. 2011). Since the systematic errors were 3%–8% for apparent radii (Güver et al. 2012b) and ~10% for touchdown fluxes (Güver et al. 2012a), we adopted 8% and 10% systematic errors for apparent radius and touchdown flux, respectively. Thus, the mean touchdown flux and apparent area are $(2.69 \pm 0.57) \times 10^{-9}$ erg s^{-1} cm^{-2} and 10.9 ± 4.4 (km/10 kpc)^2 for these PRE bursts. We note that two PRE bursts were observed by *EXOSAT* with peak fluxes $(1.0 \pm 0.1) \times 10^{-8}$ erg s^{-1} cm^{-2} and touchdown fluxes of about $(2.2–4.2) \times 10^{-9}$ erg s^{-1} cm^{-2} (Sztajno et al. 1987). The touchdown flux observations of *RXTE* and *EXOSAT* for 4U 1746-37 were consistent with each other. It should be mentioned that Sztajno et al. (1987) treated the peak flux as the Eddington flux. Here we adopted the touchdown flux as its Eddington flux as suggested in Özel et al. (2009).

4U 1746-37 has a high system inclination angle ($i \sim 90^\circ$). In such systems, the touchdown fluxes were systematically smaller than the peak fluxes. Galloway et al. (2008b) found that the ratios between the peak flux ($F_{\rm p}$) and the touchdown flux ($F_{\rm TD}$) are larger than ~1.6 in dipping binaries. They discussed two geometric interpretations of this ratio, the reflection of the far-side accretion disk and the obscuration of the near-side accretion

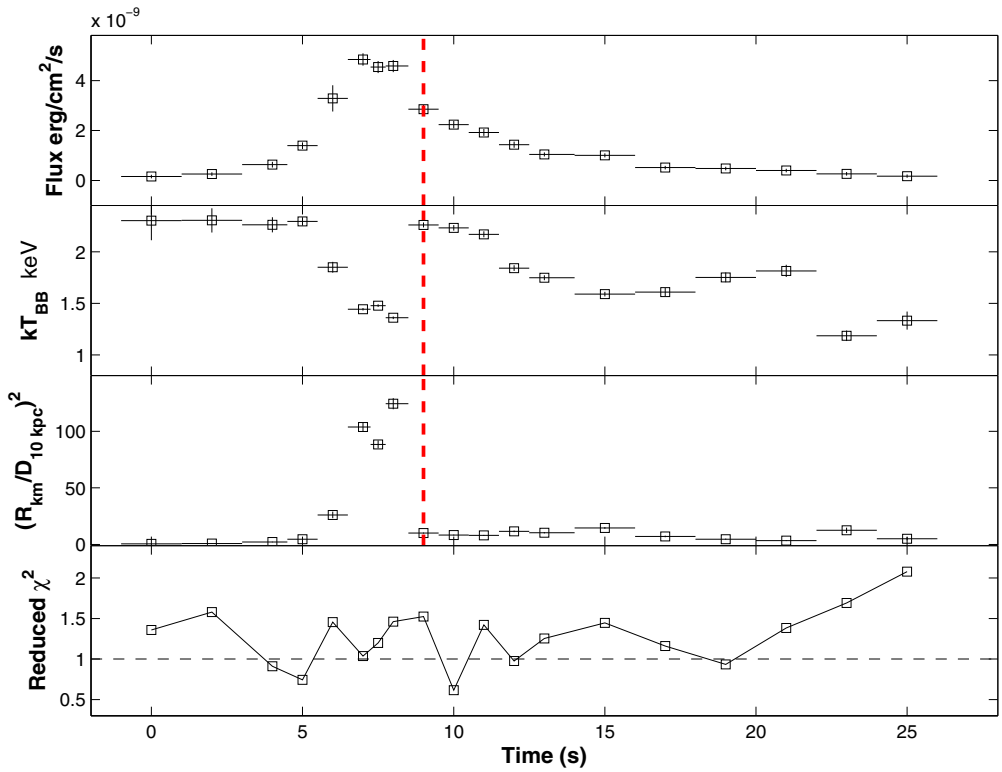

Figure 2. Time-resolved spectra of PRE burst in 4U 1746-37 (ObsID 30701-11-03-000). The red dashed line labels the touchdown moment. The 1σ errors are displayed. For some data, the errors are smaller than the symbols.

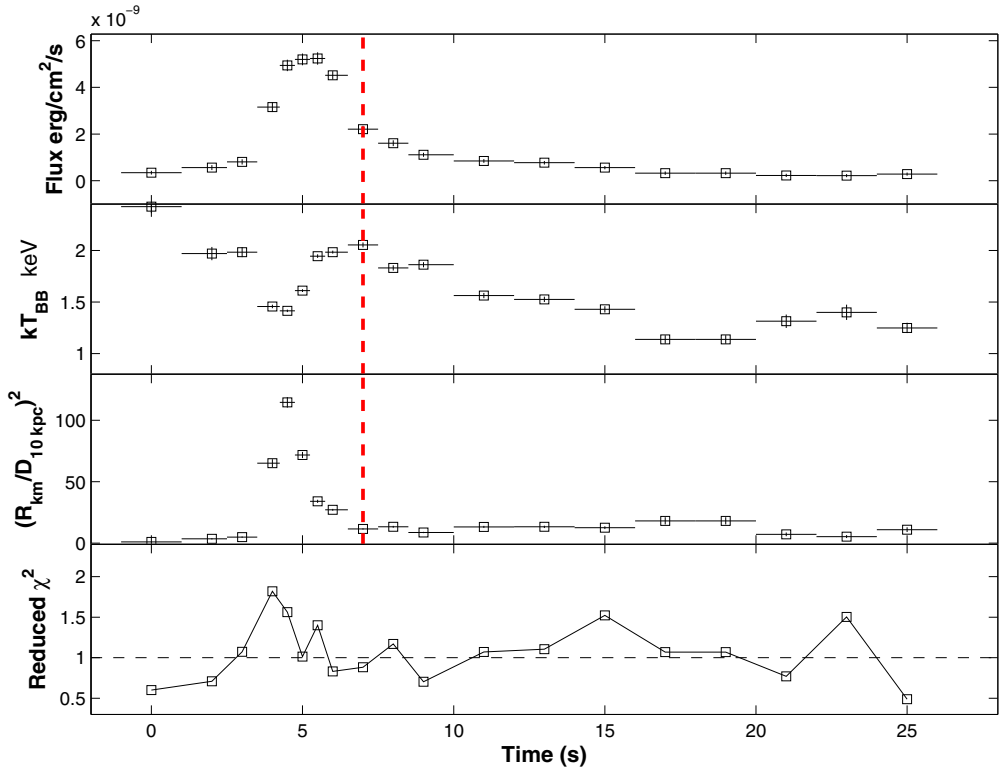

Figure 3. Time-resolved spectra of PRE burst in 4U 1746-37 (ObsID 30701-11-04-00).

disk. For the first scenario, the difference between $F_{\rm p}$ and $F_{\rm TD}$ is due to the extra contribution from the far-side disk reflection at the peak flux moment. Thus, the touchdown flux exactly corresponds to its Eddington flux. For the second scenario, it is the anisotropies of persistent and burst emission, which have been discussed for a long time (Lapidus & Sunyaev 1985; Fujimoto 1988; Zamfir et al. 2012). If the geometrically thin accretion disk extends close to the NS surface, it will intercept

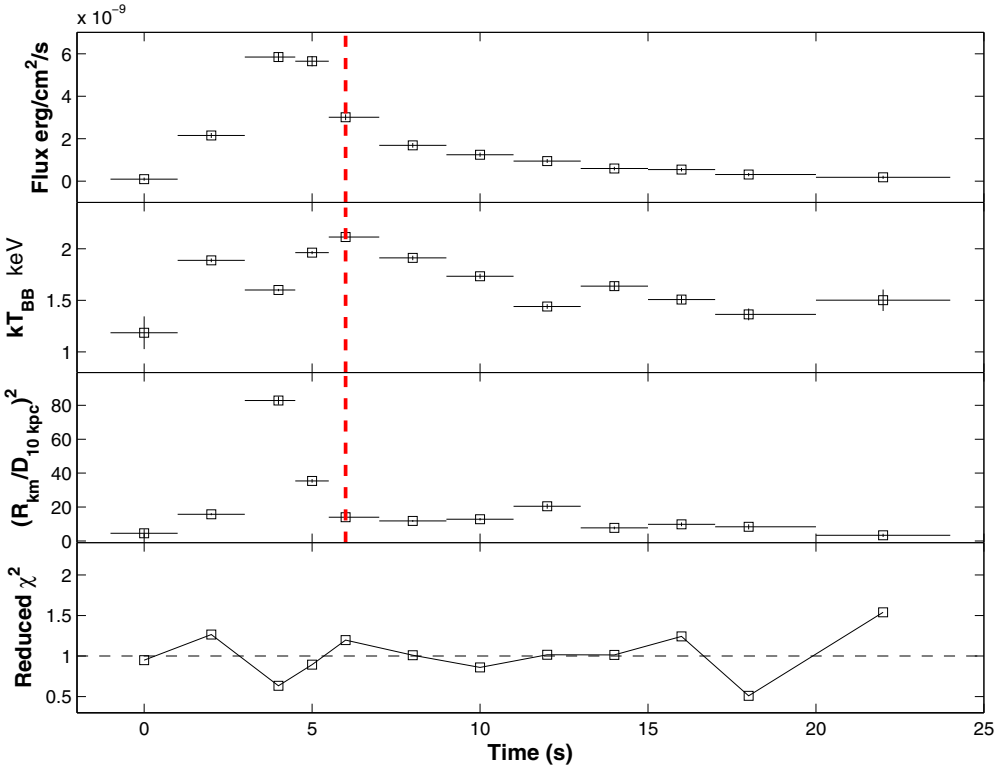

Figure 4. Time-resolved spectra of PRE burst in 4U 1746-37 (ObsID 60044-02-01-03).

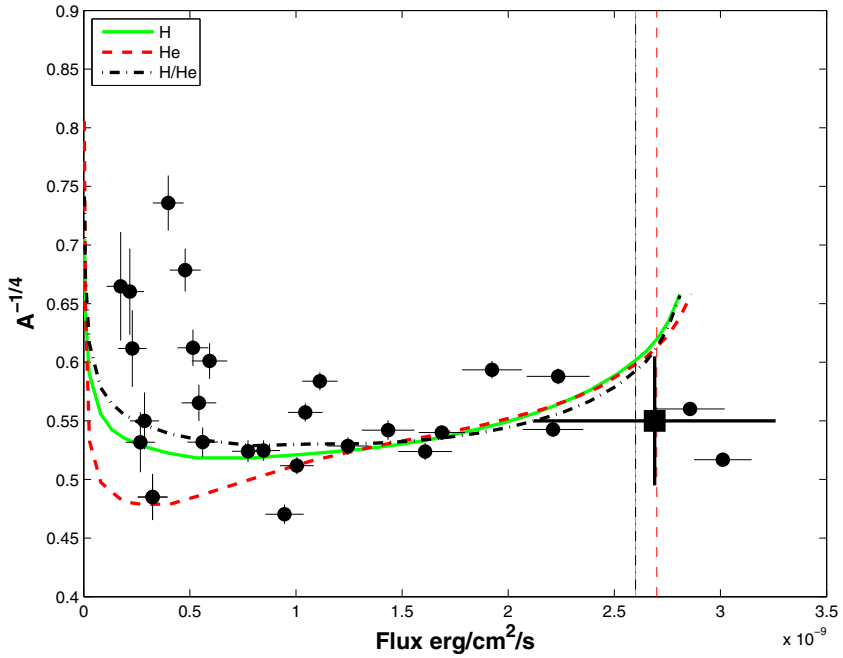

Figure 5. Evolution curve of $A^{-1/4}$. Suleimanov et al. (2011) suggested that it reflects the variation of the color correction factor during the cooling tail. Three theoretical models for $\log g = 14$ (g is the gravitational constant) and $R = 14.8$ km are displayed by the solid green curve (pure hydrogen), red dashed curve (pure helium), and black dot–dashed curve (solar mixture of H/He with metal abundance of $Z = 0.01\ \ Z_{\odot}$; Suleimanov et al. 2012), which are able to fit the data at high flux (i.e., larger than 0.5×10^{-9} erg s^{-1} cm^{-2}). However, the models cannot fit the data well at low flux. The vertical lines mark the Eddington fluxes for the aforementioned theoretical model prediction, displayed with the same line styles. Note that these theoretical curves are calculated for a particular mass and radius of NSs. The black square shows the 1σ confidence interval of the Eddington flux and cooling area measured from the touchdown method.

$\sim 1/4$ of the burst radiation and reradiate along the disk axis (Lapidus & Sunyaev 1985). Fujimoto (1988) introduced an anisotropy parameter ξ and expressed the actual luminosity of burst emission as $L = 4\pi D^2 \xi F_{\rm b}$, where $F_{\rm b}$ is the observed burst flux. Lapidus & Sunyaev (1985) suggested the approximate approach for ξ:

$$\xi^{-1} = \frac{1}{2} + |\cos i|. \quad (5)$$

In an edge-on binary system, the anisotropy parameter ξ is 2. Moreover, it can be estimated as $F_{\rm p}/F_{\rm TD}$, since theobscured

fraction of burst emission at the peak flux moment is much smaller than the one at the touchdown moment (Galloway et al. 2008b). Hence, in this circumstance, the touchdown flux and emission area in the cooling tail should be corrected to larger values with the factor $F_{\rm p}/F_{\rm TD}$. Here $F_{\rm p}/F_{\rm TD}$ is 2.0 ± 0.3 for 4U 1746-37, which is consistent with the above-mentioned prediction. We considered these two geometric effects separately.

3. THE CONSTRAINING OF M AND R

In PRE bursts, the mass and radius of NSs are constrained from the relations (Özel et al. 2009)

$$F_{\rm TD}=\frac{GMc}{k_{\rm es}D^2}\left(1-\frac{2GM}{Rc^2}\right)^{1/2} \quad (6)$$

and

$$A=\frac{R^2}{D^2 f_{\rm c}^4}\left(1-\frac{2GM}{Rc^2}\right)^{-1}, \quad (7)$$

where $k_{\rm es}=0.2(1+X)\,{\rm cm^2\ g^{-1}}$ is the opacity to electron scattering and $f_{\rm c}$ is the color correction factor. In order to constrain the mass and radius of NSs properly, the uncertainties of photosphere composition (X), distance, and the color correction factor should be taken into account together. Özel et al. (2009) proposed a Bayesian framework to estimate the mass and radius of NSs. They set each quantity with independent probability distribution functions, and then the joint probability density of mass and radius is expressed as

$$P(D,X,f_{\rm c},M,R)=\frac{1}{2}|J\left(\frac{F_{\rm TD},A}{M,R}\right)|P(D)P(X)\\ P(f_{\rm c})P(F_{\rm TD})P(A)dDdXdf_{\rm c}dMdR, \quad (8)$$

where the Jacobian of the transformation from the pair $(F_{\rm TD},A)$ to (M,R) is supposed to be

$$J\left(\frac{F_{\rm TD},A}{M,R}\right)=\frac{2GcR}{k_{\rm es}D^4 f_c^4}\left(1-4\frac{GM}{Rc^2}\right)\left(1-\frac{2GM}{Rc^2}\right)^{-3/2}. \quad (9)$$

Özel et al. (2012) made a correction for this expression compared to Equation (9) in Özel et al. (2009), but a factor of two is still missing. However, the mass–radius confident regions are not affected by the constant factor in Equation (8) when the joint probability density is normalized. Integrating Equation (8) over distance, the joint probability distribution of M and R is obtained.

In this work a Monte Carlo method is applied to constrain M and R of NSs, which shows high efficiency (Li et al. 2012). We produce two series of simulated $F'_{\rm TD}$ and A', which satisfy $F'_{\rm TD}\sim N(F_{\rm TD,obs},\sigma^2_{F_{\rm TD}})$ and $A'\sim N(A_{\rm obs},\sigma^2_A)$, respectively. Here $N(F_{\rm TD,obs},\sigma^2_{F_{\rm TD}})$ denotes that $F'_{\rm TD}$ is a normally distributed random value with expectation $F_{\rm TD,obs}$ and standard deviation $\sigma_{F_{\rm TD}}$. $N(A_{\rm obs},\sigma^2_A)$ has a similar definition. We also assign flat distributions for X, $f_{\rm c}$, which are correspondingly represented as $X'\sim U[X-dX,X+dX]$, $f'_{\rm c}\sim U[f_{\rm c}-df_{\rm c},f_{\rm c}+df_{\rm c}]$. Especially, the distance to the source has asymmetric errors. In order to simplify the simulation, we adopt $D'\sim\{N(D_0,\sigma^2_{D_1})1_{[D_0,\infty)}(D)+N(D_0,\sigma^2_{D_2})1_{(-\infty,D_0)}(D)\}$, where $1_{[D_0,\infty)}(D)$ denotes the indicator function of set $[D_0,\infty)$, $D_0=11$ kpc, $\sigma_{D_1}=0.9$ kpc, and $\sigma_{D_2}=0.8$ kpc.[6] The hydrogen mass fraction and the color correction factor are set as 0.35 ± 0.35 and 1.35 ± 0.05, respectively (Suleimanov et al. 2011; Güver et al. 2012b). For each pair of $(F'_{\rm TD},A',D',f'_{\rm c},X')$, the M and R of NSs are solved from Equations (6) and (7), if the solutions exist. For certain large samples (i.e., 10^7), the confidence regions of M and R are obtained.

4. RESULTS

We applied a Monto Carlo simulation to constrain the mass and radius of NSs in 4U 1746-37. The typical distributions of the color correction factor and hydrogen mass fraction were utilized. The results are shown in Figures 6 and 7. The left panel in Figure 6 displays the 1σ, 2σ, and 3σ confidence regions of the mass and radius of 4U 1746-37, if the touchdown flux exactly corresponds to the Eddington flux. That is, the peak flux contained a significant fraction component from the reflection of the far-side disk. If the accretion disk obscured a portion of emission area at the touchdown moment and in the cooling tail, $F_{\rm TD}$ and A should be corrected with the factor $F_{\rm p}/F_{\rm TD}$; here, the factor 2.0 ± 0.3 was adopted. The confidence regions are displayed in the left panel of Figure 7. Ten EoSs are also plotted. It should be mentioned that in each case two regions are preferred. In Figure 6, the mass and radius of NSs are $0.63\pm0.18\,M_\odot$ and 2.14 ± 0.61 km for the upper left part, or $0.21\pm0.06\,M_\odot$ and 6.26 ± 0.99 km for the lower right part. In Figure 7, the mass and radius of NSs are $0.99\pm0.29\,M_\odot$ and 3.55 ± 1.14 km for the upper left part, or $0.41\pm0.14\,M_\odot$ and 8.73 ± 1.54 km for the bottom right part.

We also checked the prior and posterior distributions of all related parameters. From Figures 6 and 7, the posterior distributions are well consistent with prior ones.

The left contours cannot be reproduced by any EoS, because the mean densities of NSs are much larger than the nuclear matter saturation density, and they are close to the Schwarzschild radius. The results show that 4U 1746-37 contains a very low-mass NS in the range 0.21–0.41 $M_\odot$. If only the reflection of the far-side disk effect existed, the touchdown flux is equal to its Eddington flux. Then, we conclude the presence of an ultra-low-mass and small-radius NS inside 4U 1746-37.

Steiner et al. (2010) proposed that the photosphere could still be extended at the touchdown moment. At the extreme case, the photosphere radius is much larger than the radius of NSs, and then the Eddington flux in Equation (6) is reduced to

$$F_{\rm TD}=\frac{GMc}{k_{\rm es}D^2}; \quad (10)$$

the expression of apparent area in Equation (7) remains unchanged. The simulation results are shown in Figures 8 and 9. Each mass of an NS corresponds to two different radius solutions. Compared with Figures 6 and 7, the left contours are shrunk in Figures 8 and 9, and the right contours are shifted negligibly.

5. DISCUSSION AND CONCLUSIONS

Plenty of theoretical NS EoSs were proposed. The hadron star and hybrid/mixed star are gravity bound and covered by crusts with nuclei and electrons, whereas the quark star and

[6] A flat distribution of D is also attempted. The M–R confidence contours are shifted negligibly.

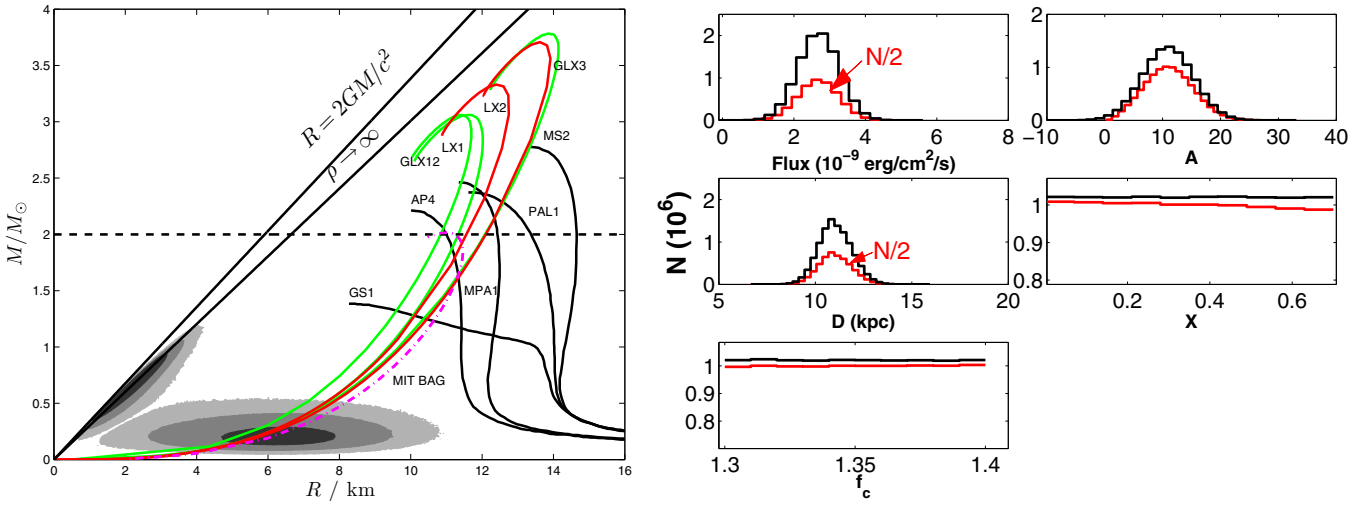

Figure 6. Left panel: 1σ, 2σ, and 3σ M–R confidence regions of 4U 1746-37, which are based on the assumption that the touchdown flux corresponded to the Eddington flux. The dashed line denotes two observed near $2\,M_\odot$ NSs. The left black lines show the general relativity limit and the central density limit, respectively. Theoretical mass–radius relations for several NS EoS models are displayed, which were introduced by GS1 (Glendenning & Schaffner-Bielich 1999), AP4 (Akmal & Pandharipande 1997), MPA1 (Müther et al. 1987), PAL1 (Prakash et al. 1988), MS2 (Müller & Serot 1996), GLX123 (Guo et al. 2014), and LX12 (Lai & Xu 2009; Lai et al. 2013). The purple dot–dashed line represents the bare strange stars obtained from the MIT bag model EoS. In order to reach $M_{\rm max}=2\,M_\odot$, the bag constant must equal 57 MeV fm^{-3}. The first five gravity-bound NSs describe the same as in Lattimer & Prakash (2007). Right panel: prior (black lines) and posterior (red lines) distributions of all relative parameters. In order to show the flux and distance distributions clearly, the total numbers of posterior distributions in both subgraphs are divided by a factor of two, because the prior and posterior distributions are quite similar. The simulation contains 10^7 samples.

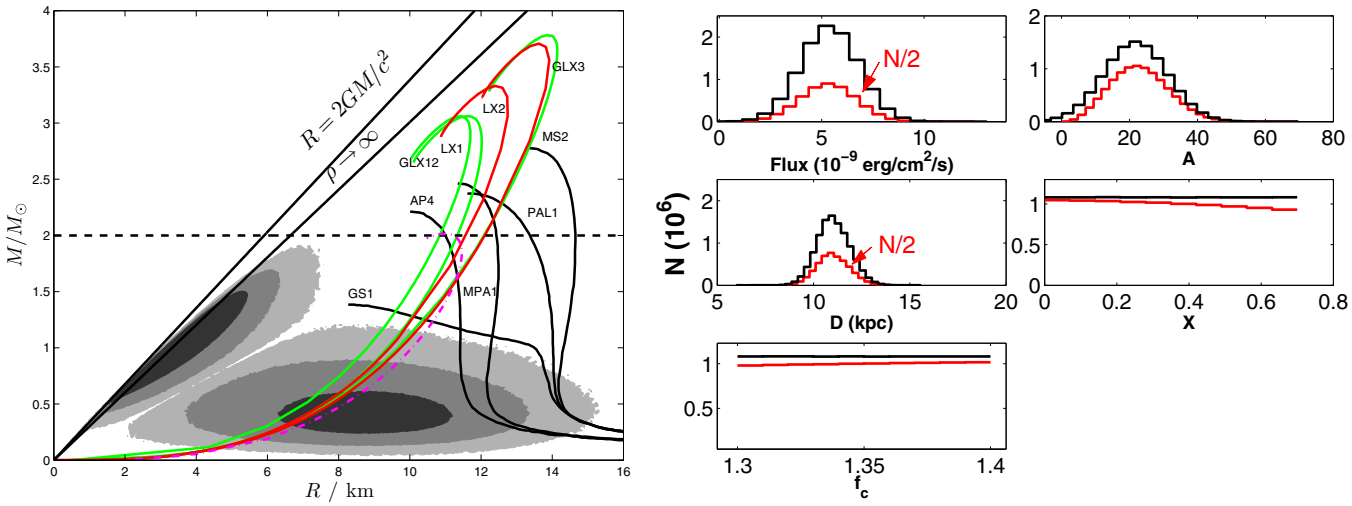

Figure 7. Same as Figure 6, but based on the assumption that the touchdown flux and emission area were partially obscured by the accretion disk. For 4U 1746-37, the obscuration factor $F_{\rm p}/F_{\rm TD}$ is 2.0 ± 0.3, and its error is accounted for in the contours of M–R.

quark-cluster star are strongly self-bound on the surface. In order to reduce them, searching for very high-mass NSs is an essential method, since the maximum mass of NSs determines the stiffness of the EoS. Very recently, the discoveries of two $\sim2\,M_\odot$ NSs ruled out all soft EoSs (Demorest et al. 2010; Antoniadis et al. 2013), in which the predicted maximum masses of NSs were lower than $2\,M_\odot$. On the other hand, searching for very low mass NSs is also an attractive method, because the EoS of self-bound NSs predicted distinct radii at low mass compared with ones by the EoS of gravity-bound NSs. Moreover, gravity-bound NSs have minimum mass, while self-bound NSs do not. Thus, theoretical NS EoSs could be effectively tested from the accurate measurement of the radius for low-mass NSs.

EXOSAT and *RXTE* observed very low touchdown fluxes in PRE bursts from 4U 1746-37 (Sztajno et al. 1987; Galloway et al. 2008a). During the cooling tail in its PRE bursts, the emission area remained nearly constant (Güver et al. 2012b). Sztajno et al. (1987) assigned the peak fluxes as its Eddington flux. However, we assume that the Eddington luminosity was reached at the touchdown moment in 4U 1746-37's PRE bursts, similar to other sources. We also checked the persistent emission variations during X-ray bursts in 4U 1746-37. The f_a model does not provide better-fitting results. After applying the Monte Carlo simulation, we propose that a low-mass NS ($0.21\pm0.06\,M_\odot$ or $0.41\pm0.14\,M_\odot$, depending on accretion disk geometric effects) may exist in 4U 1746-37. Combining the above two possibilities, the mass of 4U 1746-37 is $0.41^{+0.70}_{-0.30}\,M_\odot$ at 99.7% confidence. The peak fluxes in PRE bursts were not always consistent with touchdown fluxes. Two geometric effects, the reflection of the far-side accretion disk and the obscuration of the near-side accretion disk, were possible attributes. In the case of accretion disk reflection, the derived mass and radius of NSs in 4U 1746-37 could be reproduced in the framework of

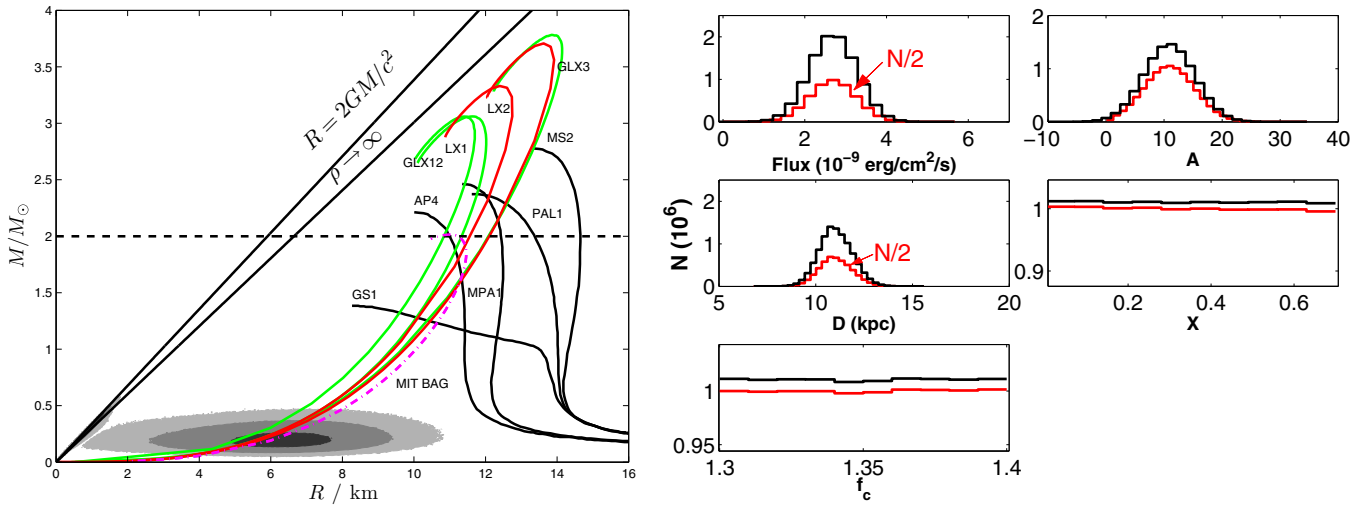

Figure 8. Same geometric effect as Figure 6. The radius of the photosphere at the touchdown moment is much larger than R.

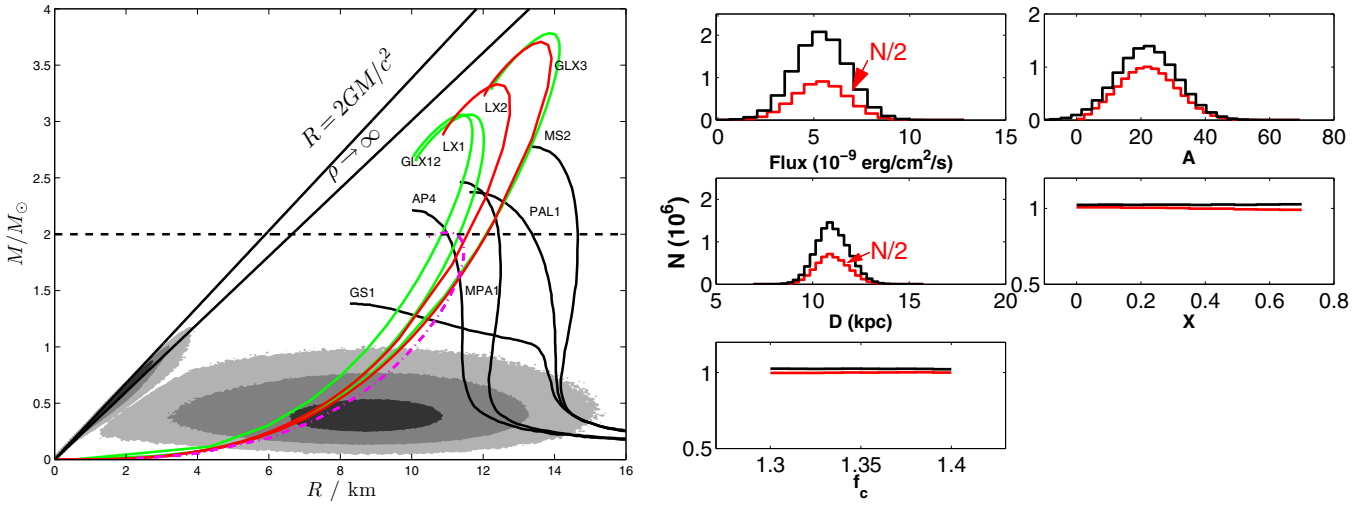

Figure 9. Same geometric effect as in Figure 7, but based on the assumption that the touchdown flux and emission area were partially obscured by the accretion disk and the photosphere is extremely extended at the touchdown moment.

self-bound NS EoSs, including quark-cluster stars and bare strange stars (Lai & Xu 2009; Lai et al. 2013; Guo et al. 2014). In the case of accretion disk obscuration, the self-bound NSs and gravity-bound NSs (Akmal & Pandharipande 1997; Müther et al. 1987) are acceptable in 1σ and 2σ confidence levels of the mass and radius of NSs in 4U 1746-37, respectively. Three gravity-bound NS EoSs (Prakash et al. 1988; Müller & Serot 1996; Glendenning & Schaffner-Bielich 1999) can survive at the 3σ confidence level.

Steiner et al. (2010) discussed the possibility that the photosphere is still extended at the touchdown moment. In the extreme case, the Eddington flux is only dependent on the stellar mass. In Figure 8, the contours of M–R constrain the same EoS as in Figure 6. Again, self-bound NSs are acceptable at the 1σ confidence level. Two gravity-bound EoSs (Akmal & Pandharipande 1997; Müther et al. 1987) and another three gravity-bound EoSs are possible at 2σ and 3σ confidence levels.

Several low-mass NSs (near or below $1\,M_\odot$) were also discovered in other binary systems, e.g., $1.07\pm0.36\,M_\odot$ for Her X-1 (Rawls et al. 2011), $1.04\pm0.09\,M_\odot$ for SMC X-1 (van der Meer et al. 2007; Rawls et al. 2011), $0.87\pm0.07\,M_\odot$ (eccentric orbit) or $1.00\pm0.01\,M_\odot$ (circular orbit) for 4U 1538-52 (Rawls et al. 2011), and $0.72^{+0.51}_{-0.58}\,M_\odot$ for PSR J1518+4904 (Janssen et al. 2008), but without radius measurement. A low-mass NS may be difficult to form from the collapse of a massive star. However, an extremely low-mass, self-bound star (strange quark or quark-cluster star), even as low as planet mass (Xu & Wu 2003; Horvath 2012), could exist through the accretion-induced collapse of a white dwarf (Xu 2005; Du et al. 2009).

The EoS of cold matter at supranuclear density, which is essentially related to the challenging nonperturbative behavior of quantum chromodynamics, is far beyond solved even nearly half a century after the discovery of pulsars. Based on different manifestations of pulsar-like compact stars (e.g., the featureless thermal X-ray spectrum and the free precession), Xu (2003) conjectured that pulsars could be so-called solid quark stars, a kind of condensed object composed of quark-cluster stars. The state of such quark-cluster matter is very stiff, and the resultant maximum mass of the quark-cluster star would be even larger than $2\,M_\odot$ (Lai & Xu 2009), which is consistent with the later discoveries of massive pulsars (Demorest et al. 2010; Antoniadis et al. 2013). Additionally, pulsar glitches (sudden spin-up) can also be well understood in the regime of the quark-cluster star model (Zhou et al. 2014).

In the conventional calculations of the crust of a strange star, one usually assumes that the bottom crust density could be as high as the drip density because the transmission probability through the Coulomb barrier is negligible for very heavy ions, e.g., $A = 118$, $Z = 36$ (Alcock et al. 1986). However, accreted matter is mostly composed of ions that are not so heavy, and the transmission probability through the Coulomb barrier could be as high as 10^{-18} for ^{16}O, according to the same approximations presented by Alcock et al. (1986). Normal matter accreted can then easily penetrate the Coulomb barrier and thus can hardly exist outside a strange quark star (a newborn strange star could be bare because of strong explosions; otherwise, a supernova might not be successful). Nevertheless, in the case of a quark-cluster star, an additional so-called strangeness barrier exists on the quark-cluster surface. Xu (2014) demonstrated that a quark-cluster star may be surrounded by a hot corona or an atmosphere, or even a crust for different accretion rates, which could be helpful to understand the O VIII Lyα emission line in 4U 1700+24 (Nucita et al. 2014). The mass of the corona or atmosphere or crust is much less than the conventional value $\sim 10^{-5}\,M_{\odot}$ of a strange star; hence, the scale is negligible compared with the radius of NSs.

On the other hand, Jaikumar et al. (2006) suggested that the strange stars may have a neutralizing solid crust consisting of charged strangelets and electrons, if the surface tension is below the critical value of order a few MeV fm^{-2} (Alford et al. 2006). Alford & Eby (2008) pointed out that the thickness of strangelet-crystal crust is sensitive to the EoS and the surface tension and can be changed from zero to hundreds of meters for a compact star of radius 10 km and mass 1.5 $M_{\odot}$, or thicker for low-mass NSs. However, the thickness of the crust does not change the radius of NSs significantly, even in the extreme case of 4U 1746-37.

As demonstrated in this paper, the mass–radius curves of various quark-cluster stars and bare strange stars pass the case of 4U 1746-37, no matter which geometric effects operated (reflection or obscuration). Certainly, our conclusions are based on the assumption that the observed PRE bursts had reached their Eddington luminosity. In future observations, if a brighter PRE burst is observed in 4U 1746-37, then a larger-mass NS is required. Moreover, we are expecting that the optical observations of the next-generation telescope, Thirty Meter Telescope (TMT, http://www.tmt.org/) could provide rigorous mass constraints. With TMT, the optical light curves and spectroscopy could be capable of obtaining the binary system information (such as inclination angle, the type of companion star, and mass function; Antoniadis et al. 2013). Then, the mass of the compact object will be measured precisely and independently, which can verify the reliability of an ultra-low-mass NS in 4U 1746-37.

This work is supported by the 973 program No. 2012CB821801 and No. 2014CB845800, the National Natural Science Foundation of China (11225314, 11173024), and the Strategic Priority Research Program on Space Science of the Chinese Academy of Sciences (XDA04010300), XTP XDA04060604. Z. S. Li is supported by China Postdoctoral Science Foundation (2014M560844). This research has made use of data obtained from the High Energy Astrophysics Science Archive Research Center (HEASARC), provided by NASA's Goddard Space Flight Center.

REFERENCES

Akmal, A., & Pandharipande, V. R. 1997, PhRvC, 56, 2261
Alcock, C., Farhi, E., & Olinto, A. 1986, ApJ, 310, 261
Alford, M. G., & Eby, D. A. 2008, PhRvC, 78, 045802
Alford, M. G., Rajagopal, K., Reddy, S., & Steiner, A. W. 2006, PhRvD, 73, 114016
Antoniadis, J., Freire, P. C. C., Wex, N., et al. 2013, Sci, 340, 448
Bednarek, I., Haensel, P., Zdunik, J. L., Bejger, M., & Mańka, R. 2012, A&A, 543, A157
Bhattacharyya, S. 2010, AdSpR, 45, 949
Demorest, P. B., Pennucci, T., Ransom, S. M., Roberts, M. S. E., & Hessels, J. W. T. 2010, Natur, 467, 1081
Du, Y. J., Xu, R. X., Qiao, G. J., & Han, J. L. 2009, MNRAS, 399, 1587
Fortin, M., Zdunik, J. L., Haensel, P., & Bejger, M. 2014, arXiv:1408.3052
Fujimoto, M. Y. 1988, ApJ, 324, 995
Galloway, D. K., Muno, M. P., Hartman, J. M., Psaltis, D., & Chakrabarty, D. 2008a, ApJS, 179, 360
Galloway, D. K., Özel, F., & Psaltis, D. 2008b, MNRAS, 387, 268
García, F., Zhang, G., & Méndez, M. 2013, MNRAS, 429, 3266
Glendenning, N. 1996, Compact Stars. Nuclear Physics, Particle Physics and General Relativity (New York: Springer)
Glendenning, N. K., & Schaffner-Bielich, J. 1999, PhRvC, 60, 025803
Guillot, S., Servillat, M., Webb, N. A., & Rutledge, R. E. 2013, ApJ, 772, 7
Guo, Y.-J., Lai, X.-Y., & Xu, R.-X. 2014, ChPhC, 38, 055101
Güver, T., Özel, F., Cabrera-Lavers, A., & Wroblewski, P. 2010a, ApJ, 712, 964
Güver, T., Özel, F., & Psaltis, D. 2012a, ApJ, 747, 77
Güver, T., Psaltis, D., & Özel, F. 2012b, ApJ, 747, 76
Güver, T., Wroblewski, P., Camarota, L., & Özel, F. 2010b, ApJ, 719, 1807
Haensel, P., Potekhin, A. Y., & Yakovlev, D. G. (ed.) 2007, in Neutron Stars 1: Equation of State and Structure (Astrophysics and Space Science Library, Vol. 326, New York: Springer)
Horvath, J. E. 2012, RAA, 12, 813
in't Zand, J. J. M., Galloway, D. K., Marshall, H. L., et al. 2013, A&A, 553, A83
in't Zand, J. J. M., Strohmayer, T. E., Markwardt, C. B., & Swank, J. 2003, A&A, 409, 659
Jaikumar, P., Reddy, S., & Steiner, A. W. 2006, PhRvL, 96, 041101
Janssen, G. H., Stappers, B. W., Kramer, M., et al. 2008, A&A, 490, 753
Kuulkers, E., den Hartog, P. R., in't Zand, J. J. M., et al. 2003, A&A, 399, 663
Lai, X. Y., Gao, C. Y., & Xu, R. X. 2013, MNRAS, 431, 3282
Lai, X. Y., & Xu, R. X. 2009, MNRAS, 398, L31
Lapidus, I. I., & Sunyaev, R. A. 1985, MNRAS, 217, 291
Lattimer, J. M. 2012, ARNPS, 62, 485
Lattimer, J. M., & Prakash, M. 2007, PhR, 442, 109
Leahy, D. A. 2004, ApJ, 613, 517
Lewin, W. H. G., van Paradijs, J., & Taam, R. E. 1993, SSRv, 62, 223
Li, Z., Chen, L., & Wang, D. 2012, PASP, 124, 297
Müller, H., & Serot, B. D. 1996, NuPhA, 606, 508
Müther, H., Prakash, M., & Ainsworth, T. L. 1987, PhLB, 199, 469
Nucita, A. A., Stefanelli, S., De Paolis, F., et al. 2014, A&A, 562, A55
Özel, F., Gould, A., & Güver, T. 2012, ApJ, 748, 5
Özel, F., Güver, T., & Psaltis, D. 2009, ApJ, 693, 1775
Prakash, M., Lattimer, J. M., & Ainsworth, T. L. 1988, PhRvL, 61, 2518
Rawls, M. L., Orosz, J. A., McClintock, J. E., et al. 2011, ApJ, 730, 25
Sala, G., Haberl, F., José, J., et al. 2012, ApJ, 752, 158
Sidoli, L., Parmar, A. N., Oosterbroek, T., et al. 2001, A&A, 368, 451
Steiner, A. W., Lattimer, J. M., & Brown, E. F. 2010, ApJ, 722, 33
Suleimanov, V., Poutanen, J., & Werner, K. 2011, A&A, 527, A139
Suleimanov, V., Poutanen, J., & Werner, K. 2012, A&A, 545, A120
Sztajno, M., Fujimoto, M. Y., van Paradijs, J., et al. 1987, MNRAS, 226, 39
Tsujimoto, M., Guainazzi, M., Plucinsky, P. P., et al. 2011, A&A, 525, A25
van der Meer, A., Kaper, L., van Kerkwijk, M. H., Heemskerk, M. H. M., & van den Heuvel, E. P. J. 2007, A&A, 473, 523
Worpel, H., Galloway, D. K., & Price, D. J. 2013, ApJ, 772, 94
Xu, R. X. 2003, ApJL, 596, L59
Xu, R. X. 2005, MNRAS, 356, 359
Xu, R.-X. 2014, RAA, 14, 617
Xu, R.-X., & Wu, F. 2003, ChPhL, 20, 806
Zamfir, M., Cumming, A., & Galloway, D. K. 2012, ApJ, 749, 69
Zhou, E. P., Lu, J. G., Tong, H., & Xu, R. X. 2014, MNRAS, 443, 2705